IranJOC

Iranian Journal of
Organic Chemistry

Crystal structure, theoretical study and mechanism investigation of stable phosphorus ylide involving 9-carbazole

Niloufar Akbarzadeh-Torbati[a*], Sayyed Mostafa Habibi-Khorassani[a], Malek Taher Maghsoodlou[a], Norollah Hazeri[a], Mohammad Zakarianezhad[b], Hamideh Saravani[a], Ali Paknahad[a], Brian W. Skelton[c] and Mohamed Makha[c]

[a]*Department of Chemistry, The University of Sistan and Baluchestan, P. O. Box 98135-674, Zahedan, Iran*
[b]*Department Of Chemistry, Faculty Of Science, Payam Noor University, Sirjan, Iran*
[c]*School of Biomedical, Biomolecular and Chemical Sciences, M310, University of Western Australia, Perth, WA 6009, Australia*

Abstract: The crystal structure of di-tert-butyl 2-(9H-carbazol-9-yl)-3-(triphenylphosphoranylidene) butanediate has been determined by X-ray crystallography. This compound crystallizes in a monoclinic space group $P2_1/n$ with cell parameters a = 17.566(3) Å, b = 12.2342(9) Å, c = 18.5561(12) Å, β = 117.818(12)°, V = 3527.0(7) Å^3, D_{calc} = 1.235 mg m^{-3}, and Z = 4. The final R value is 0.0463 for 12602 reflections. Mechanistic investigation of the reaction between di-tert-butyl acetylenedicarboxylate and triphenylphosphine in the presence of 9-carbazol as a N-H heterocyclic compound was fully discussed. In addition assignment of the stability of the two Z- and E- isomers of ylide involving 9-carbazole have been performed using quantum mechanical calculations.

Introduction

Phosphorus ylides have been found in a wide variety of reactions of interest to synthetic chemists, especially in the synthesis of naturally occurring products and compounds with biological and pharmacological activity [1-2]. The development of the modern chemistry of natural products and physiologically active compounds would have been impossible without the phosphorus ylides. Such compounds have attained great significance as widely used reagents for linking synthetic building blocks with the formation of carbon-carbon double bonds.

In continuation of our research based upon investigation of the chemistry of P-ylides [3-5], an X-ray analysis of synthesized ylide involving 9-carbazole, quantum mechanical calculations along with mechanism investigation were undertaken and its crystal structure determined with the inherent conformation established.

*Corresponding author. Tel: (+98) 541 8052301, Fax: (+98) 541 2446565, E-mail: n.akbarzadeh@chem.usb.ac.ir

Results and discussion

X-ray crystallography:

Stable phosphorus ylide **4** was synthesized from the reaction between di-*tert*-butyl acetylenedicarbocxylate, triphenylphosphine and carbazole as a N-H heterocyclic compound (Figure **15**) [6]. The molecular structure of compound **4c**, showing the atom numbering scheme is presented in Figure **1** and its molecular packing is indicated in Figure **2**.

Crystallographic data and the refinement procedures are given in Table **1** and selected bond lengths, bond angles, and torsion angles of **4c** are also listed in Table **2**. As can be seen, there is a good agreement between crystallographic and theoretical data.

On the basis of obtained result from X-ray crystallography, it is obvious that adjacent carbonyl group in the ylide moiety of compound **4c** ($C_{921}=O_{921}$, see Figure **1**) has a resonance with bond of $C_{92}=P_1$. In the present work, single crystal X-ray diffraction of

stable phosphorus ylide **4c** was prepared from solution involving 95% of one isomer. Herein, X-ray analysis data exhibit the *Z*-structure for this compound, because of the *tert*-butoxy group along with triphenylphosphine are placed in the same side of carbon-carbon double bond (See Figure **15-j**).
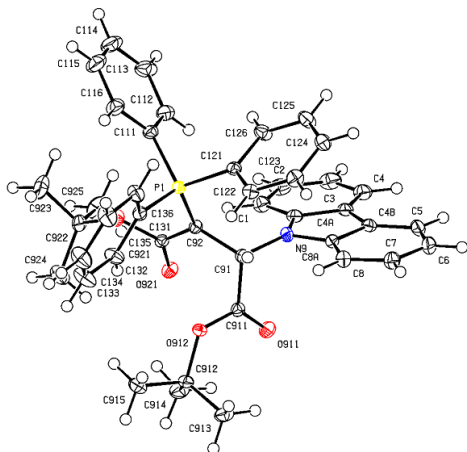

Figure 1: ORTEP view of the molecular geometry of phosphorus ylide **4**. Ellipsoids have been drawn at the 50% probability level. Hydrogen atoms have been omitted for clarity.
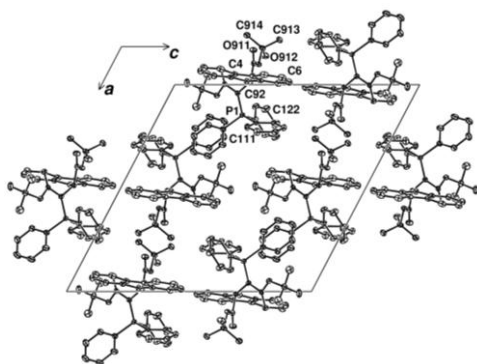

Figure 2: The molecular packing diagram of phosphorus ylide **4c**.

Table 1: Crystal data and structure refinement for compound **4c**.

Empirical formula	$C_{42}H_{42}NO_4P$
Formula weight	655.74
Temperature	100(2) K
Crystal system	Monoclinic
Space group	$P2_1/n$
Unit cell dimensions	a = 17.566(3) Å
	b = 12.2342(9) Å
	c = 18.5561(12) Å
	β = 117.818(12)°
Volume	3527.0(7) Å^3
Z	4
Density (calculated)	1.235 g cm^{-3}

Absorption coefficient	0.121 mm^{-1}
Crystal size	0.38 x 0.31 x 0.25 mm^3
θ range for data collection	2.85 to 33.10°.
Index ranges	-26<=h<=26, -13<=k<=18, -27<=l<=28
Reflections collected	44988
Independent reflections	12602 [R(int) = 0.0482]
Max./ min. Transmission	0.97/ 0.96
Refinement method	Full-matrix least-squares on F^2
Data / restraints / parameters	12602 / 0 / 439
Goodness-of-fit on F^2	0.903
Final R indices [$I>2\sigma(I)$]	$R_1 = 0.0463$, $wR_2 = 0.1015$
R indices (all data)	$R_1 = 0.0783$, $wR_2 = 0.1073$
Largest diff. peak and hole	0.485 and -0.344 e.Å^{-3}
CCDC	760456

On the other hand, ^{1}H NMR spectroscopic data exhibited that *tert*-butoxy group is shielded due to the anisotropic effect of a phenyl group in compound **4c** containing triphenylphosphine and must be appeared at the high filed. The ^{1}H NMR spectrum of ylide **4c** exhibited two signals at 0.98 and 1.52 ppm arising from the two *tert*-butoxy groups for the *Z*-isomer. The *tert*-butoxy group at 0.98 ppm in the *Z*-isomer is a result of the anisotropic effect. This effect confirms why the *Z*- and *E*- isomers could be appeared as the major and minor forms, respectively. With respect to the obtained result from crystallographic data, the report of our previous work [6], should be corrected and major form should be reported for the *Z*-isomer of ylide **4c** or other ylides.

Theoretical calculation:

For assignment of the two *Z*- and *E*- isomers as a major or minor form in phosphorus ylides **4(a, c)** containing a carbazole, the *Z*- and *E*- isomers were optimized for all ylide structures at HF/6-31G(d,p) level of theory [7] by Gaussian03 package program [8]. The relative stabilization energies for both the geometrical isomers have been calculated at B3LYP/6-311++G(d,p) level. Atoms in molecules (AIM) [9] and the calculation of charge on the atoms by natural population analysis (NPA) [10] and CHelpG keyword at HF/6-31G(d,p) level of theory have been performed in order to gain a better understanding of the most geometrical parameters in both the *E*-**4(a, c)** and the *Z*-**4(a, c)** of phosphorus ylides Figure **15**. The numbers of critical points and intramolecular hydrogen bonds as well as the charge of atoms that constructed on the *Z*-

and *E-* isomers have been recognized. The results altogether reveal the effective factors on stability of *Z-* and *E-* ylide isomers. Relative stabilization energy of the two isomers has been calculated at HF/6-31G(d,p) and B3LYP/6-311++G(d,p) levels (See Figures **3** and

5). The relative stabilization energies for the two isomers [*Z-***4(a, c)** and *E-***4(a, c)**] are reported in Table **3**, as can be seen, the *Z-***4a** and the *Z-***4c** isomers are more stable than the *E-***4a** and *E-***4c** forms (2.45 and 1.83kcal/mol, respectively) at B3LYP level.

Table 2: Selected Bond Lengths (Å), Bond Angles (°) and Torsion Angles for compound **4c**.

Bond Lengths	(Å)	Bond Angles	(°)	Torsion Angles	(°)
C(91)-C(92)	1.514(2)a	N(9)-C(91)-C(92)	116.8[a](1)	N(9)-C(91)-C(92)-P(1)	-92.6[a](1)
	[1.521][b]		[117.0][lb]		[-84.81][b]
	[1.515][c]		[118.2][c]		[-87.34][c]
C(92)-C(921)	1.421(2)	C(91)-C(911)-O(911)	123.8(1)	P(1)-C(92)-C(921)-O(921)	-177.5(1)
	[1.428]		[123.7]		[-179.0]
	[1.427]		[124.5]		[-180.0]
C(921)-O(921)	1.230(1)	C(911)-C(91)-C(92)	114.1(1)	P(1)-C(92)-C(921)-O(922)	2.4(1)
	[1.209]		[114.4]		[0.5]
	[1.122]		[114.9]		[1.2]
C(921)-O(922)	1.373(2)	C(92)-C(921)-O(921)	125.6(1)		-13.3(2)
	[1.345]		[125.2]	O(921)-C(921)-C(92)-C(91)	[-4.90]
	[1.331]		[122.3]		[-8.69]
O(922)-C(922)	1.464(1)		119.0(1)	O(911)-C(911)-C(91)-C(92)	132.6(1)
	[1.446]	C(91)-C(92)-C(921)	[119.9]		[128.6]
	[1.450]		[126.6]		[123.31]
	1.541(2)	C(921)-C(92)-P(1)	120.69(9)	C(4)-C(4a)-C(4b)-C(5)	1.8(3)
C(91)-C(911)	[1.537]		[118.64]		[0.03]
	[1.537]		[122.37]		[0.02]
C(911)-O(911)	1.205(1)	C(92)-C(921)-O(922)	111.8(1)	C(91)-N(9)-C(8a)-C(8)	-12.7(2)
	[1.209]		[112.9]		[-3.63]
	[1.186]		[111.52]		[-1.3]
C(911)-O(912)	1.339(1)				13.3(2)
	[1.346]			C(91)-N(9)-C(9a)-C(1)	[2.5]
	[1.325]				[2.8]
O(912)-C(912)	1.489(2)				1.2(2)
	[1.446]			C(2)-C(1)-C(9a)-C(4a)	[1.2]
	[1.450]				[1.1]
	1.724(1)				0.8(2)
C(92)-P(1)	[1.735]			C(7)-C(8)-C(8a)-C(4b)	[2.80
	[1.742]				[1.4
C(91)-N(9)	1.468(1)				27.7(1)
	[1.460]			C(131)-P(1)-C(121)-C(122)	[29.2]
	[1.463]				[28.5]
				C(131)-P(1)-C(121)-C(126)	-157.5(1)
					[-150.4]
					[-152.3]

a X-ray crystaiiography data

b On the basis of theoretical calculation at HF/6-31G(d,p) level for the Z-4c isomer.

c On the basis of theoretical calculation at HF/6-31G(d,p) level for the E-4c isomer.

Table 3: The relative energy (kcal/mol) for for the two Z and E isomers of ylides **4a** and **4c**, obtained at HF/6-31G (d,p) and B3LYP/6-311++G(d,p) levels.

Conformer	HF	B3LYP
Z-4a	0.00	0.00
E-4a	3.95	2.45
Z-4c	0.00	0.00
E-4c	2.39	1.83

Further investigation was undertaken in order to determine more effective factors on stability of the two *Z*- and *E*- isomers, on the basis of AIM calculations at HF/6-31G(d,p) level of theory by the AIM2000 program package [11]. In recent years, AIM theory has often applied in the analysis of H-bonds. In this theory, the topological properties of the electron density distribution are derived from the gradient vector field of the electron density $\rho(r)$ and on the Laplacian of the electron density $\nabla^2\rho(r)$. The Laplacian of the electron density, $\nabla^2\rho(r)$, identifies regions of space wherein the electronic charge is locally depleted $[\nabla^2\rho(r) > 0]$ or built up $[\nabla^2\rho(r) < 0]$. Two interacting atoms in a molecule form a critical point in the electron density, where $\nabla\rho(r) = 0$, called the bond critical point (BCP). The values of charge density and its Laplacian at these critical points give useful information regarding the strength of the H-bonds [11]. The ranges of $\rho(r)$ and $\nabla^2\rho(r)$ are (0.002–0.035) e/a_0^3 and (0.024–0.139) e/a_0^5, respectively, if H-bonds exist [12]. The AIM calculation indicates intramolecular hydrogen bonds and critical points (H-BCP) for the two *Z*-**4(a, c)** and *E*-**4(a, c)** isomers. Intramolecular H-BCPs are shown in Figures **1** and **2** (dotted line). The electron densities (ρ), Laplacian of electron density $\nabla^2\rho(r)$, and energy density -H(r) are also reported in Tables **4** and **5**. A negative total energy density at the BCP reflects a dominance of potential energy density, which is the consequence of accumulated stabilizing electronic charge [13]. Herein, the number of hydrogen bonds in both categories (*E*-**4a** and *Z*-**4a**) and (*E*-**4c** and *Z*-**4c**) are (8 and 7) and (13 and 11), respectively. The values of ρ and $\nabla^2\rho(r)$ are in the ranges (0.005-0.021 and 0.008-0.020) e/a_0^3, (0.029-0.090 and 0.029-0.079) e/a_0^5 and (0.024-0.090 and 0.029-0.079) e/a_0^5, respectively. In addition the Hamiltonian [-H(r)] is in the range (0.0010-0.0021 and 0.0008-0.0022 au) and (0.0010-0.0022 and 0.0008-0.0022 au) (See Tables **4** and **5**). These HBs show $\nabla^2\rho(r) > 0$ and H(r) < 0, which according to classification of Rozas *et al*. [14] are medium-strength hydrogen bonds. In both ylides the dipole moment for the two *E*-**4a** and *E*-**4c** isomers (3.51 and 4.03 D, respectively) are smaller than the two *Z*-**4a** and *Z*-**4c** isomers (6.81 and 6.83 D, respectively) and the value of -H$_{tot}$ (=$\sum$H(r)) for the two *Z*-**4a** and *Z*-**4c** isomers (97.87 and 164.93 au, respectively) are smaller than the two *E*-**4a** and *E*-**4c** isomers (116.51 and 201.28 au, respectively). Although, dipole moment, the number of hydrogen bonds and -H$_{tot}$ in both of the E-**4(a-c)**, taken altogether (see Table **6**), appear as three factors on stability of the E-**4(a-c)**,

but these values are not adequte reseans to provide a powerfull effect as a dominance of potential energy. It seems that other factor i.e. other intractions exception of H-BCPS intractions and anisotropic effect of a phenyl group in **4a** or **4c** compounds containing triphenylphosphine for the two Z-**4c** and Z-**4a** could be accounted against mention factors for changing the order of relation energy between the Z- and E-isomers (see Table **3**). As expected, according to theoretical calculations the relative energy at both levels, are compatible with the experimental results from the X-ray, ^{1}H, ^{13}C and ^{31}P NMR spectroscopy which indicat the Z-**4a** is more abundance isomer. Moreover, the total number of hydrogen bonds in the two Z-**4c** and E-**4c** (13, 11) are more than the two Z-**4a** and E-**4a** (8, 7), this leads to a large rigidity in these geometrical isomers in comparison with the two Z-**4a** and E-**4a** forms. The rigidity of the two molecular structures by the very large intramolecular hydrogen bonds accompanied by more steric factor of the bulky tert-bulky groups (compare with dimethy groups in both the *E*-**4a** and Z-**4a**, Figures **3** and **4**) within the structures (*E*-**4c** and Z-**4c** forms) make a good opportunity for enhancement of energy barrier. Hence, interconversion process between the two isomer needs to pass through a very high restricted barrier energy, particular in solution media, for this reason it is possible to see only a single isomer as a lone isomers of **4c** (Z-**4c**) (Figure **5**). On the contrary, interconversion process for both the *E*-**4a** and Z-**4a** geometrical isomers pass through a considerably low energy barrier, which leads to a plausible observation of the two *E*-**4a** and Z-**4a** [See Figure **15-j**]. In the synthesis of ylides **4a** and **4c**[6], the ^{1}H, ^{13}C, ^{31}P NMR data showed a lone isomer of **4c** with the most abundance percentage of Z-4c isomer as a major form and also a mixture of the two *E*-**4a** and Z-**4a** isomers.
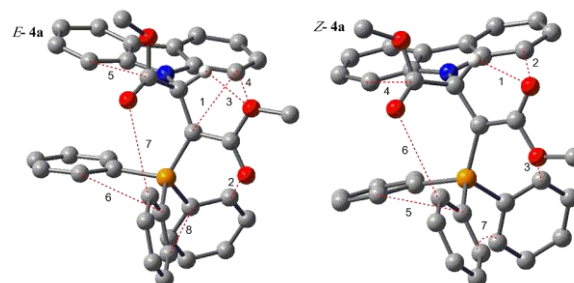

Figure 3: H-Bond length bonds (dotted lines) in the two *E*-**4a** and Z-**4a** geometrical isomers of stable ylide **4a**.

Also, the charge on different atoms which are calculated by NPA and AIM methods and also CHelpG keyword at HF/6-31G(d,p) level are reported in Table

7 for the two *Z*- and *E*- isomers of ylides **4a** and **4c**. There is a good agreement between the results in three methods. The differences between the charge on C_1 atoms (for example) in relation to the Z-**4a** and E-**4a** and also Z-**4c** and E-**4c** in three methods are very close to each other.
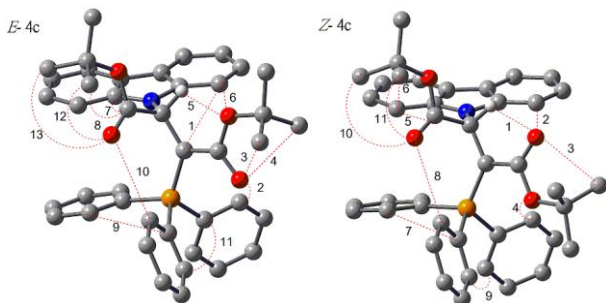

Figure 4: Intramolecular H-Bond length hydrogen bonds (dotted lines) in the *two E*-**4c** and *Z*-**4c** geometrical isomers of stable ylide **4c.**

Kinetics:

Kinetics parameters involving rate constant and activation energy for ylides 4a,4b and 4c have been earlier reported [15]. Herein, effect of concentration and machanism investigation (Figure **16k**) of these reactions as a complementary study were fully discussed. UV spectra of all reactants (compounds **1**, **2** and **3**) along with products (**4c**) are shown in Figures **6**, **7**, **8** and **9** respectively.

Table 4: The values of $\rho \times 10^3$, $\nabla^2\rho \times 10^3$ and Hamiltonian $(-H) \times 10^4$ for both the Z-**4a** and the E-**4a** isomers of ylide **4a** calculated at the hydrogen bond critical points. All quantities are in atomic units.

E	ρ	$\nabla^2\rho$	-H	Z	ρ	$\nabla^2\rho$	-H
1	7.21	27.71	12.64	1	19.48	78.51	10.57
2	10.30	41.81	12.84	2	9.22	35.12	8.88
3	20.67	89.23	16.27	3	8.30	35.35	13.99
4	5.44	24.49	11.42	4	10.12	43.59	22.03
5	10.81	45.24	21.16	5	8.30	29.84	14.92
6	8.66	31.60	15.46	6	12.60	50.57	10.78
7	13.05	52.28	10.59	7	9.52	35.14	16.61
8	9.30	33.47	16.13				

Table 5: The values of $\rho \times 10^{-3}$, $\nabla^2\rho \times 10^{-3}$ and Hamiltonian $(-H) \times 10^{-4}$ for the two *Z*-**4c** and *E*-**4c** isomers of ylide **4c** calculated at the hydrogen bond critical Points. All quantities are in atomic units.

E	ρ	$\nabla^2\rho$	-H	Z	ρ	$\nabla^2\rho$	-H
1	7.21	27.69	12.67	1	19.56	78.38	10.07
2	10.32	41.88	12.84	2	9.24	35.16	8.84
3	15.65	67.21	16.75	3	16.57	68.68	17.22
4	16.09	67.85	17.70	4	8.33	35.54	14.17
5	20.76	89.31	15.89	5	10.07	43.90	22.18
6	5.46	24.64	11.61	6	9.24	38.54	22.33
7	10.77	45.55	21.21	7	8.30	29.85	14.92
8	9.41	38.90	22.27	8	12.66	50.61	10.59
9	8.66	31.58	15.44	9	9.52	35.14	16.62
10	13.11	52.31	10.39	10	14.19	60.98	16.17
11	9.30	33.47	16.12	11	16.19	63.01	11.82
12	14.47	61.84	16.75				
13	16.14	62.68	11.64				

Effect of concentration:

To determine reaction order with respect to triphenylphosphine **1** and dialkyl acetylene-dicarboxylate **2** (in fact **2c**), in a series of other separate experiments**,** all kinetic studies were carried out in the presence of excess **3** (**3a** or **3b**). Under this condition the rate equation may be expressed as:

$$rate = k_{obs}[1]^\alpha [2]^\beta, \qquad k_{obs} = k_2 [3]^\gamma \qquad \text{or}$$

$$Ln\, k_{obs} = Ln\, k_2 + \gamma\, Ln[3] \qquad (1)$$

In this case (3×10^{-2} M of **3a** instead of 3×10^{-3} M) using the original experimental absorbance versus time data provides a second order fit curve (solid line) against time at 355 nm which exactly fits the experimental curve. The value of rate constant was the same as with that of obtained from the previous experiment (3×10^{-3} M). Repeating the experiments with 5×10^{-2}M and 7×10^{-2}M of **3a** gave separately the same fit curve and rate constant. In fact, the experimental data indicated that the observed pseudo second order rate constant (k_{obs}), was equal to the second order rate

constant (k_2), this is possible when γ is zero in equation (1). It is appears, therefore, that the reaction is zero and second order with respect to **3** (NH-acid) and the sum of **1** and **2** ($\alpha + \beta = 2$), respectively. To determine reaction order with respect to dialkyl acetylenedicarboxylate **2** (**2c**), a separate experiment was performed in the presence of excess of **1**

$$\text{rate} = k'_{obs} [3]^{\gamma} [2]^{\beta}, \qquad k'_{obs} = k_2 [1]^{\alpha}$$
(2)

Table 6: The most important geometrical parameters involving the value of -H_{tot}/au, dipole moment/D and the number of hydrogen bonds for the two *Z*- and *E*- isomers of ylides **4a** and **4c**.

Isomer	-H_{tot}/au	dipole moment/D	number of H-BCPS
E-**4a**	116.51	3.51	8
Z-**4a**	97.87	6.81	7
E-**4c**	201.28	4.03	13
Z-**4c**	164.93	6.83	11

Table 7: The charges on different atoms for both *Z* and *E* isomers in both ylides **4a** and **4c** calculated by AIM, CHelpG and NBORead respectively method at HF/6-31g(d,p)

number of atom	Z-4a	E-4a	Z-4c	E-4c
C1	2.69×10^{-1} [a] (0.05) [b] (-0.44) [c]	2.60×10^{-1} (0.01) (-0.47)	2.86×10^{-1} (0.12) (-0.43)	3.08×10^{-1} (0.23) (-0.43)
C2	-7.72×10^{-1} (-0.44) (-0.83)	-8.54×10^{-1} (-0.44) (-0.84)	-7.63×10^{-1} (-0.48) (-0.83)	-7.37×10^{-1} (-0.51) (-0.83)
C4	1.85 (0.89) (0.91)	1.88 (0.88) (0.92)	1.88 (0.92) (0.91)	1.87 (0.96) (0.91)
O5	-1.38 (-0.65) (-0.76)	-1.42 (-0.74) (-0.79)	-1.41 (-0.66) (-0.76)	-1.42 (-0.76) (-0.76)
O6	-1.30 (-0.44) (-0.66)	-1.28 (-0.37) (-0.63)	-1.31 (-0.65) (-0.69)	-1.30 (-0.62) (-0.69)
P3	3.23 (0.26) (1.75)	3.24 (0.23) (1.75)	3.25 (0.29) (1.75)	3.24 (0.29) (1.75)

a) Calculated by AIM method
b) Calculated by CHelpG method
c) Calculated by NBORead method

The original experimental absorbance versus time data is shown in Figure **10**. These data provide a pseudo first order fit curve at 355 nm, which exactly fits the experimental curve (dotted line) as shown in Figure **11**.

As a result, since $\gamma = 0$ (as determined previously), it is reasonable to accept that the reaction is first order with respect to compound **2c** ($\beta = 1$). Because the overall order of reaction is two ($\alpha + \beta + \gamma = 2$) it is obvious that $\alpha = 1$ and the order of triphenylphosphine

1 must be equal to one. Based on the above results, a simplified proposed reaction mechanism (Figure **15-k**)
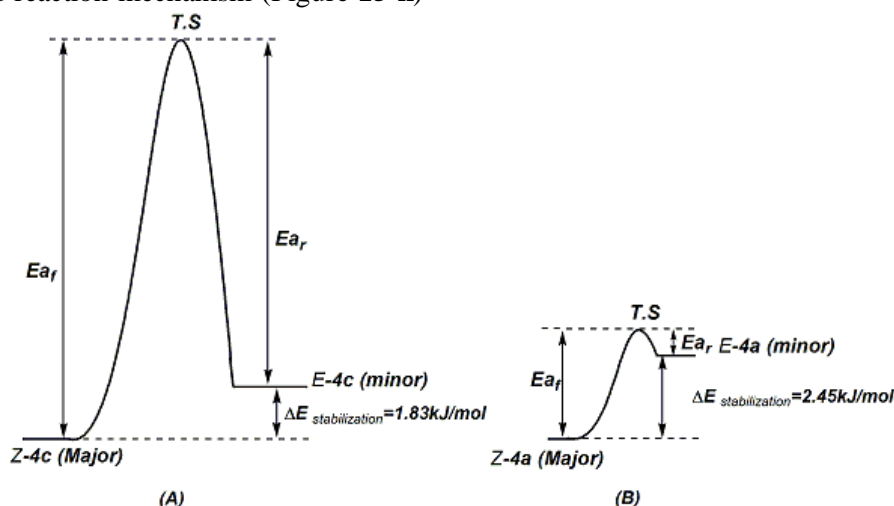

Figure 5: Interchangeable process of geometrical isomers for ylides 4a and 4c (A) A very high restricted barrier energy for interconversion process between the two *E*-4c and *Z*-4c isomers. (B) A low high restricted barrier energy for interconversion process between the two *E*-4a and *Z*-4a isomers.
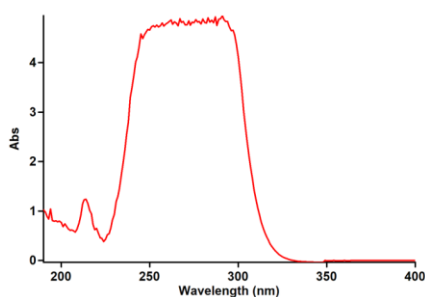

 Figure 6: The UV spectrum of 10^{-3}M triphenyl-phosphine 1 in CCl_4.

Figure 7: The UV spectrum of 10^{-3}M di-*tert*-butyl acetylenedicarboxylate **2c** in CCl_4.

The experimental results indicate that the third step (rate constant k_3) is possibly fast. In contrast, it may be assumed that the third step is the rate-determining step for the proposed mechanism. In this case, the rate law can be expressed as follows:

$$rate = k_3 [I_1][3] \quad (3)$$

The steady-state assumption can be employed for $[I_1]$ that is generated following equation,

is shown in Figure **12.**

$$[I_1] = \frac{k_2[1][2]}{k_{-2} + k_3[3]}$$

The value of $[I_1]$ can be replaced in equation (3) to obtain equation (4):

$$rate = \frac{k_2 k_3 [1][2][3]}{k_{-2} + k_3 [3]} \quad (4)$$

Since it was assumed that k_3 is relevant to the rate-determining step, it is reasonable to make the following assumption: $k_{-2} \gg k_3 [3]$ so the rate low becomes:
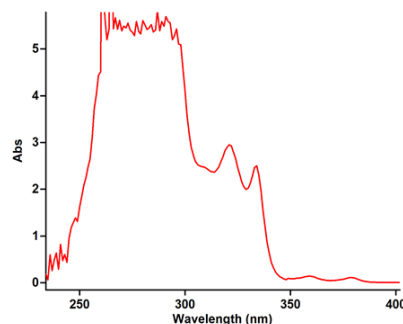
$$rate = \frac{k_2 k_3 [1][2][3]}{k_{-2}} \quad (5)$$

Figure 8: The UV spectrum of 10-3M Carbazole 3 in CCl_4.

The final equation indicates that the overall order of reaction is three which is not compatible with the experimental overall order of reaction (=two). In addition, according to this equation, the order of reaction with respect to carbazole **3** is one, whereas it was actually shown to be equal to zero. For this reason, it appeared that third step is fast. If we assume that the fourth step (rate constant k_4) is the rate-determining step for the proposed mechanism, in this case, there are

two ionic species to consider in the rate-determining step namely phosphonium ion (I_2) and Carbazole ion (N^-).
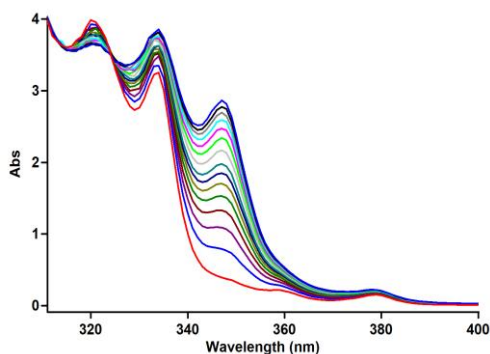

Figure 9: The UV spectra of the reaction between 10^{-3} M of each compounds **1**, **2c** and **3** as reaction proceeds in CCl_4.
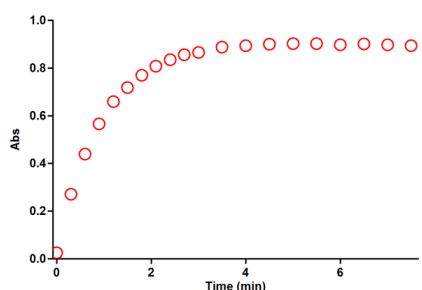

Figure 10: The absorbance change *versus* time for the reaction between **2c** and **3** in the presence of excess **1** (10^{-2}M) at 355 nm and -5.0˚C in CCl_4.
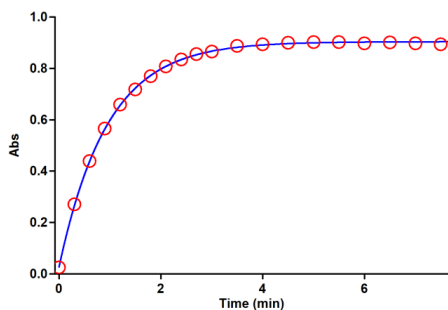

Figure 11: Pseudo first order fit curve (solid line) for the reaction between **2c** and **3** in the presence of excess **1** (10^{-2} M) at 355 nm and -5.0˚C in CCl_4.
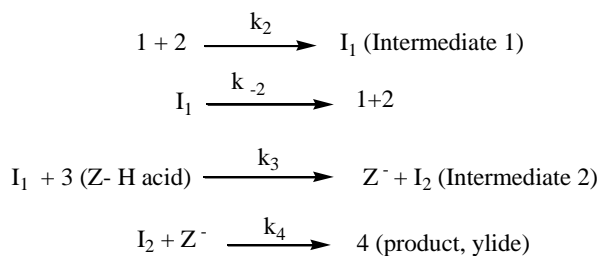

Figure 12: The simplified scheme for the proposed reaction mechanism.

The phosphonium and carbazole ione, as we see in Figure **15-k**, have full positive and negative charges and form very powerful ion-dipole bonds to the 1,2-dichloromethane, the high dielectric constant solvent. However, the transition state of the reaction between the two ions carries a dispersed charge, which here is divided between the attacking carbazole and the phosphonium ions. Bonding of solvent (1,2-dichloromethane) to this dispersed charge, would be much weaker than to the concentrated charge of carbazole and phosphonium ions. The solvent thus would stabilize the ionic species more than it does in the transition state, and therefore E_a would be higher, slowing down the reaction. However, in practice, 1,2-dichloromethane speeds up the reaction, and for this reason, the fourth step, which is independent of the change in the solvent medium, could not be the rate-determining step. Furthermore, the rate law of formation of the product (fourth step) for a proposed reaction mechanism with application of steady-state assumption can be expressed by: $rate = k_4 [I_2][N^-]$

By application of steady-state for [I^-] and [N^-], and replacement of their values in the above equation, the equation (6) is obtained:

$$rate = \frac{k_2 k_3 [1][2][3]}{k_{-2} + k_3 [3]} \quad (6)$$

This equation is independent of the rate constant for the fourth step (k_4) and shows why the fourth step would not be affected by a change in the solvent medium. In addition, it has been suggested earlier that the kinetics of ionic species˙ phenomena (e.g., the fourth step) are very fast [16-18]. If the first step (rate constant k_2) were the rate determining-step, in this case, two reactants (triphenylphosphine **1** and dialkyl acetylenedicarboxylate **2**), as we see (Figure **15-k**), have no charge and could not form strong ion-dipole bonds to the high dielectric constant solvent, dichloromethane.However, the transition state carries a dispersed charge which here is divided between the attacking **1** and **2** and, hence bonding of solvent to this dispersed charge is much stronger than to the reactants, which lack charge. The solvent thus stabilizes the transition state more than it does the reactans, and therefore E_a is reduced which speeds up the reaction. Our experimental results, show that the solvent with the higher dielectric constant exerts a powerful effect on the rate of reaction (in fact, the first step has rate constant k_2 in proposed mechanism) but the opposite occurs with the solvent of lower dielectric constant (CCl_4, see Tables **7**, **8** and **9**). The results of the current work (effects of solvent and concentration of compounds, in particular, the concentration of NH-

acids) have provided useful evidence for steps 1 (k_2), 3 (k_3) and 4 (k_4) of the reactions between triphenylphosphine **1**, dialkyl acetylenedicarboxylates **2** (**2a**, **2b** or **2c**) and carbazole **3**. Two steps involving 3 and 4 are not rate determining, although the discussed effects, taken altogether, are compatible with the first step (k_2) of the proposed mechanism and would allow it to be the rate-determining step. However, a good kinetic description of the experimental results using a mechanistic scheme based upon the steady-state approximation is frequently taken as evidence of its validity. By application of this, the rate formation of product **4** from the reaction mechanism (Figure **12**) is given by:

$$\frac{d[4]}{dt} = \frac{d[ylide]}{dt} = rate = k_4[I_2][N^-] \quad (7)$$

We can apply the steady-state approximation to $[I_1]$ and $[I_2]$;

$$\frac{d[I_1]}{dt} = k_2[1][2] - k_{-2}[I_1] - k_3[I_1][3]$$

$$\frac{d[I_2]}{dt} = k_3[I_1][3] - k_4[I_2][N^-]$$

To obtain a suitable expression for $[I_2]$ to put into equation (7) we can assume that, after an initial brief period, the concentrations of $[I_1]$ and $[I_2]$ achieve a steady-state with their rates of formation and rates of disappearance just balanced. Therefore, $\frac{d[I_1]}{dt}$ and $\frac{d[I_2]}{dt}$ are zero and we can obtain expressions for $[I_2]$ and $[I_1]$ as follows:

$$\frac{d[I_2]}{dt} = 0 \quad [I_2] = \frac{k_3[I_1][3]}{k_4[N^-]} \quad (8)$$

$$\frac{d[I_1]}{dt} = 0 \quad , \quad [I_1] = \frac{k_2[1][2]}{k_{-2} + k_3[3]} \quad (9)$$

We can now replace $[I_1]$ in the equation (8) to obtain this equation;

$$[I_2] = \frac{k_2 k_3[1][2][3]}{k_4[N^-][k_{-2} + k_3[3]]}$$

The value of $[I_2]$ can be put into equation (7) to obtain the rate equation (10) for the proposed Mechanism:

$$rate = \frac{k_2 k_3 k_4[1][2][3][N^-]}{k_4[N^-][k_{-2} + k_3[3]]} \quad \text{or} \quad rate = \frac{k_2 k_3[1][2][3]}{[k_{-2} + k_3[3]]}$$

(10)

Since experimental data have indicated that steps 3 (k_3) and 4 (k_4) are fast but step 1 (k_2) is slow, it is therefore reasonable to make the following assumption:

k_3 [3] >> k_{-2} so the rate equation becomes:

$$rate = k_2[1][2] \quad (11)$$

This equation, which was obtained from a mechanistic scheme (shown in Figure **12**) by applying the steady-state approximation, is compatible with the results obtained by UV spectrophotometery.

Effect of structure of dialkyl acetylenedicarboxylates:

To confirm the above observations, further experiments were performed with diethyl acetylenedicarboxylate **2b** and dimethyl acetylenedicarboxylate **2a** respectively under the same conditions used in the previous experiments. The values of the second-order rate constant (k_2) for the reactions between (**1**, **2b** and **3**) and (**1**, **2a** and **3**) are reported in Tables **8** and **9** respectively for all solvents and temperatures investigated. The original experimental absorbance curves (dotted line) accompanied by the second order fit curves (full line), which exactly fit the experimental curve (dotted line), are shown in Figures **13** and **14** at -5.0 °C and 355 nm respectively.

As can be seen from Tables **8** and **9** the behavior of diethyl acetylenedicarboxylate **2b** or dimethyl acetylenedicarboxylate **2a** are the same as for di-*tert*-butylacetylenedicarboxylate **2c** with respect to the reaction with triphenylphosphine **1** and carbazole **3**. The rate of both the former reactions (**1**, **2b** and **3** or **1**, **2a** and **3**) were also accelerated in a higher dielectric constant environment and with higher temperatures, however these rates under the same conditions are approximately 8 to 10 times more than for the reaction with di-*tert*-butyl acetylenedicarboxylate **2c** (see Tables **8** and **9**). It seems that both inductive and steric factors for the bulky alkyl groups in **2b** and **2c** tend to reduce the overall reactions rate (see equation IX). In the case of dimethyl acetylenedicarboxylates **2a** or diethyl acetylenedicarboxylates **2b**, the lower steric and inductive effects of the dimethyl or diethyl groups, exert a powerful effect on the rate of reactions.

Conclusion

Herein, we investigated sterochemistry of ylide **4c** again (previously was reported) on the basis of X-ray studies to establish true isomer. The obtained results exhibited that more abundance isomer in ylide **4c** as a typical is Z-isomer with a major form. The assignment of the Z- and E- isomers as a major or minor form in both the ylides **4a** and **4c** were undertaken by AIM and NPA methods and also CHelpG keyword. Quantum mechanical calculation used to clarify how the ylides

4a and **4b** exist in solution as a mixture of the two geometrical isomers with emphasizing of major form an Z-isomer. These studies showed that why **4c** compound could be appeared as the Z-**4c** isomer in accord with major form. This result was in good agreement with the experimental data obtained from ^{1}H NMR and X-ray crystallography techniques.

Table 8: The values of second order rate constant for the reaction between **1**, **2b** and **3** in the presence of solvents such as, CCl_4, mixture of solvents (50/50%) and dichloromethane respectively at all temperatures investigated.

4	solvent	ε	k_2/M.min			
			-5.0ºC	0.0ºC	5.0ºC	10.0ºC
	CCl_4	2.02	359.3	419.5	510.4	626.4
4b	Ethyl acetate	6.02	370.74	442.23	535.73	654.18
	1,2-dichloroethane	8.93	474.63	554.07	659.13	779.75

Table 9: The values of second order rate constant for the reaction between **1**, **2a** and **3** in the presence of solvents such as, CCl_4, mixture of solvents and dichloromethane respectively at all temperatures investigated.

4	solvent	ε	k_2/M.min			
			-5.0ºC	0.0ºC	5.0ºC	10.0ºC
	CCl_4	2.02	447.5	586.4	648.2	799.2
4a	Ethyl acetate	6.02	661.4	780.95	887.17	1005.14
	1,2– dichloromethane	8.93	791.33	1003.18	1209.32	1521.5

Table 10: The values of second order rate constant for the three reactions (**1, 2c** and **3**) in the presence of different

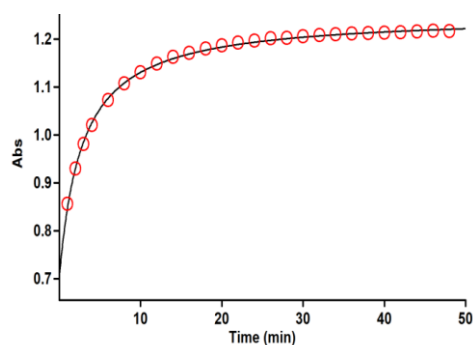| 4	solvent	ε	k_2/M.min			
			-5.0ºC	0.0ºC	5.0ºC	10.0ºC
	CCl_4	2.02	45.82	61.05	78.37	122.46
4c	Ethyl acetate	6.02	85.72	104.58	127.93	164.32
	1,2-dichloroethane	8.93	122.96	158.72	191.01	212.76

Figure 13: Second order fit curve (solid line) accompanied by the original experimental curve (dotted line) for the reaction between compounds **1, 2b** and **3** at 355 nm in CCl_4.

Kinetics investigation of the reactions between triphenylphosphin and dialkyl acetylenedicaroxylates,

in the presence of carbazole were undertaken using UV spectrophotometery. The results can be summarized as follows:

1. Effect of concentrations as a complementary study were fully discussed along with temperature and solvents effects for determination of mechanism reaction, herein, increased stric bulk in structure of the dialkyl acetylenedicarboxylates accompanied by the correspondingly greater inductive effect, reduced the overall reactions rate.

2. With respect to the experimental data, the first step of proposed mechanism was recognized as a rate-determining step (k_2) and this was confirmed based upon the steady-state approximation.

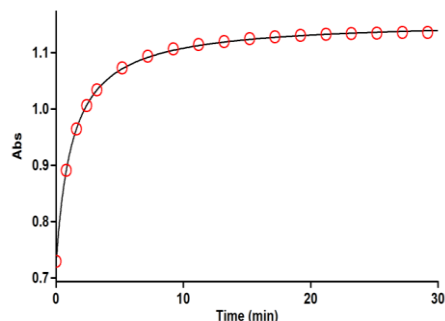**3.** Third step (k_3) is known as a fast step.

Figure 14: Second order fit curve (solid line) accompanied by the original experimental curve (dotted line) for the reaction between compounds **1, 2a** and **3** at 355 nm in CCl$_4$.

Experimental

Material and Methods:

Stable phosphorus ylide **4** was synthesized from the reaction between di-tert-butyl acetylenedicarbocxylate, triphenylphosphine and carbazole as a N-H heterocyclic compound (Figure **15**) [6].
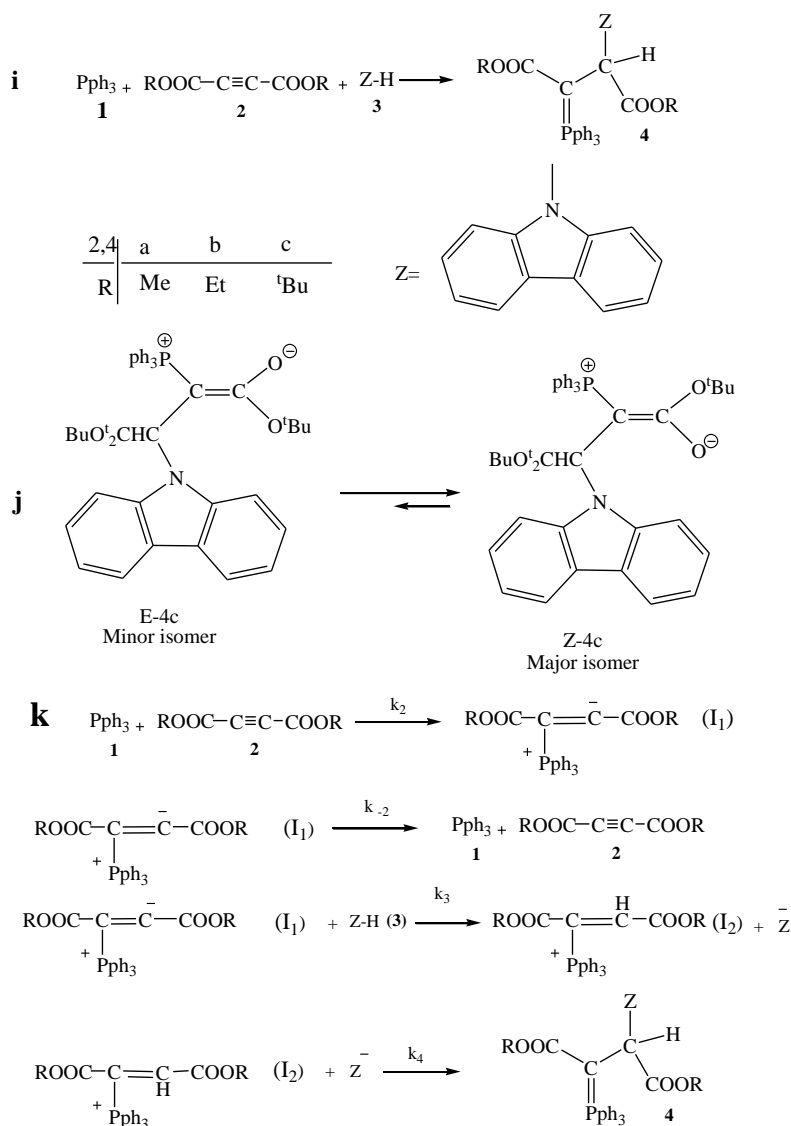

Figure 15: The reaction between triphenylphosphine **1**, dialkyl acetylenedicarboxylates **2** (**2a**, **2b** and **2c**) and carbazole **3** for generation of stable phosphorus ylides **4** (**4a**, **4b and 4c**). **j)** The two *Z*-**4c** and *E*-**4c** isomers (Major and Minor, respectively) of ylide **4c**.

Quantum mechanical calculation has been performed by Gaussian 03 program [8] and using the AIM2000 program packages [19]. Melting points and IR spectra was measured on an Electrothermal 9100 apparatus and a Shimadzu IR-470 spectrometer, respectively. The ^{1}H, ^{13}C, and ^{31}P NMR spectra were recorded on a

Bruker DRX-500 AVANCE instrument with $CDCl_3$ as a solvent at 500.1, 125.8, and 202.4 MHz, respectively. A Cary UV/vis spectrophotometer model Bio-300 with a 10 mm light-path black quartz spectrophotometer cell was employed throughout the current work. The single crystals were grown from a $CHCl_3/Et_2O$ solution. The X-ray diffraction measurements of compound **4c** were made on an Oxford Diffraction Gemini diffractometer 100K (Mo-Kα radiation, graphite monochromator, λ = 0.71073 Å). The structure of **4c** was solved by direct methods and refined by full matrix least squares on F2 (SHELXL-97) [20]. Absorption correction, data collection, cell refinement and data reduction have been carried out using Oxford Diffraction Ltd [21-22] ORTEP (molecular graphics), and WinGX (publication material) [24]. CCDC 760456 contains the supplementary crystallographic data for this paper. These data can be obtained free of charge from the Cambridge Crystallographic Data Center. Copies of the data can be obtained, free of qcharge, on application to CCDC, 12 Union Road, Cambridge CB2 1EZ, UK, (fax: +44-(0)1223-336033, e-mail: deposit@ccdc.cam.ac.uk), or via www.ccdc.cam.ac.uk/data_request/cif.

Dialkyl acetylenedicarboxylate, triphenylphosphine and 9-carbazole were purchased from Fluka (Buchs, Switzerland) and used without further purification. All extra pure solvents including dichloromethane, 1, 2-dichloroethane and THF also obtained from Merck (Darmstadt, Germany).

Acknowledgment

References

[1] Shen. Y. *Acc. Chem. Res*. **1998**, *32*, 584.

[2] Corbridge. D.E.C. *Phosphorus. An Outline of Its Chemistry, Biochemistry and Uses,* 5th edn, Elsevier, Amsterdam, **1995**.

[3] Yavari. I.; Adib. M.; Hojabri. L. *Tetrahedron* **7213**, *58*, 2002.

[4] Maghsoodlou. M. T.; Hazeri. N.; Habibi-Khorasani. S. M.; Nassiri. M.; Adhamdoust. S. R.; Salehzadeh. J. *J. Chem. Res*. **2008**. *2*, 79.

[5] Habibi-Khorassani. S. M.; Ebrahimi. A.; Maghsoodlou. M. T.; Saravani. H.; Zakarianezhad. M.; Ghahramaninezhat. M.; Kazemian. M. A.; Nassiri. M.; Khajehali. Z. *Progress in reaction kinetics and mechanism.* **2009**, *34*, 261.

[6] Habibi-Khorassani. S. M.; Maghsoodlou. M. T.; Hazeri. N.; Nassiri. M.; Marandi. Gh.; Ghulame Shahzadeh. A.

Phosphorus, Sulfur, and Silicon and the Relat. Elem. **2006**, *181*, 567.

[7] Reed. A. E.; Weinstock. R. B.; Weinhold. F. *J. Chem. Phys*. **1985**, *83*, 735.

[8] Frisch, M. J.; Trucks. G. W.; Schlegel. H. B.; Scuseria. G. E.; Robb. M. A.; Cheeseman. J. R; Montgomery. J. A.; Vreven. T.; Kudin. K. N.; Burant. J. C.; Millam. J. M.; Iyengar. S. S.; Tomasi. J.; Barone. V.; Mennucci. B.; Cossi. M.; Scalmani. G.; Rega. N.; Petersson. G. A.; Nakatsuji. H.; Hada. M.; Ehara. M.; Toyota. K.; Fukuda. R.; Hasegawa. J.; Ishida. M.; Nakajima. T.; Honda. Y.; Kitao. O; Nakai. H.; Klene. M.; Li. X.; Knox. J. E.; Hratchian. H. P.; Cross. J. B.; Adamo. C.; Jaramillo. J.; Gomperts. R.; E.Stratmann. R.; Yazyev. O.; Austin. A. J.; Cammi. R.; Pomelli. C.; Ochterski. J. W.; Ayala. P. Y.; Morokuma. K.; Voth. G. A.; Salvador. P.; Dannenberg. J. J.; Zakrzewski. V. G.; Dapprich. S.; Daniels. A. D.; Strain. M. C.; Farkas. O.; Malick. D. K.; Rabuck. A. D.; Raghavachari. K.; Foresman. J. B.; Ortiz.; J. V; Cui. Q.; Baboul. A. G.; Clifford. S.; Cioslowski. J.; Stefanov. B. B.; Liu. G.; Liashenko. A.; Piskorz. P.; Komaromi. I.; Martin. R. L.; Fox. D. J.; Keith. T.; Al-Laham. M. A.; Peng. C. Y.; Nanayakkara. A.; Challacombe. M.;. Gill. P. M. W.; Johnson. B.; Chen. W.; Wong. M. W.; Gonzalez. C.; Pople. J. A.; Gaussian 03, Revision A.1, Gaussian, Inc., Pittsburgh PA. **2003**.

[9] Bader. R. F.W. Atoms in molecules A Quantum Theory, Oxford University, New York. **1990.**

[10] Suresh, C. H.; Gadre, S. R. *J. Inorg. Chem*. **2007**, *111*, 710.

[11] Biegler König. F. W.; Schönbohm. J.; Bayle. D. *J. Comput. Chem.* **2001**. *22*, 545.

[12] Grabowski. S. J. *J. Mol. Struct*. **2001**. *562*, 137.

[13] Arnold. W. D.; Oldfield. E. *J. Am. Chem. Soc*. **2000**. *122,* 12835.

[14] Rozas. I.; Alkorta. I.; Elguero. J. *J. Am. Chem. Soc*. **2000**. *122*, 11154.

[15] Habibi-Khorassani. S. M.; Maghsoodlou. M. T.; Ebrahimi. A.; Roohi. H.; Dasmeh. H. R.; Zakarianezhad. M.; Moradian. M.; *Phosphorus, Sulfur, and Silicon and the Relat. Elem.* **2006**. *181*, 1103.

[16] Okubo. T.; Meeda. Y; Kitano. J. *J. Phys. Chem.* **1989**. *93*, 3721.

[17] Treglon. P. A.; Laurence. G. S.; *Sci. Instrum*. **1956**, *42*, 869.

[18] Wolff. M.A. *Chem. Instrum.* **1976.** *5*, 59.

[19] AlcamÍ, MÓ.; M, M.; Yáñez. *Theo. Comput. Chem.* **1996**, *3*, 407.

[20] Sheldrick. G. M.; *Acta Cryst*. **2008**. *A64*, 112.

[21] Oxford Diffraction, CrysAlis CCD, Oxford Diffraction LTD, Abingdon, England. **2006**.

[22] Oxford Diffraction, CrysAlis RED, Oxford Diffraction LTD, Abingdon, England. **2006**.

[23] Johnson. C. K.; ORTEPII, Report ORNL-5138, Oak Ridge National Laboratory, Tennessee, **1976**.

[24] Farrugia. L. J. *J. Appl. Cryst*. **1999**. *32*, 837.